NANO LETTERS

Letter

pubs.acs.org/NanoLett

Ultralight Three-Dimensional Boron Nitride Foam with Ultralow Permittivity and Superelasticity

Jun Yin, Xuemei Li, Jianxin Zhou, and Wanlin Guo*

State Key Laboratory of Mechanics and Control of Mechanical Structures, Key Laboratory for Intelligent Nano Materials and Devices of the Ministry of Education, and Institute of Nanoscience, Nanjing University of Aeronautics and Astronautics, Nanjing 210016, China

Supporting Information

ABSTRACT: Dielectrics with ultralow permittivity within 2 times that of air, excellent mechanical performance, and high thermal stability are highly attractive to many applications. However, since the finding of silica aerogels in the 1930s, no alternative ultralight porous dielectric with density below 10 mg/cm^3 has been developed. Here we present three-dimensional hierarchical boron nitride foam with permittivity of 1.03 times that of air, density of 1.6 mg/cm^3, and thermal stability up to 1200 °C obtained by chemical vapor deposition on a nickel foam template. This BN foam exhibits complete recovery after cyclic compression exceeding 70% with permittivity within 1.12 times that of air. Gathering all these exceptional characters, the BN foam should create a breakthrough development of flexible ultralow-permittivity dielectrics and ultralight materials.

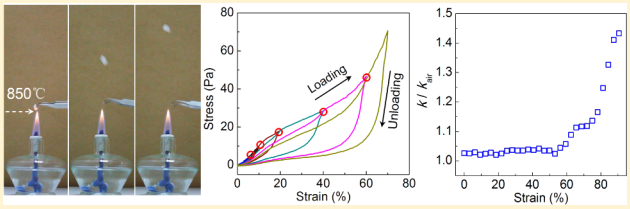

KEYWORDS: *Ultralight, ultralow permittivity, superelasticity, three-dimensional, boron nitride, aerogels*

Setting the dielectric constant of vacuum at 1, an insulating substance with $k < 2$ has been widely recognized as ultralow-k dielectric. Porous materials are not only light in weight but also necessary to extend the dielectrics well into the ultralow-k region.[1] Since the first production in 1931 by Kistler,[2] silica aerogel has been well developed as the lightest solid capable to efficiently insulate heat and electricity.[3] Recently, carbon-based conductive ultralight materials are reported with density ranging from a few to tens of micrograms per cubic centimeter.[4−9] Metallic frames consisting of hollow-tube microlattices[10] have also been successfully fabricated with density down to 0.9 mg/cm^3. These carbon- or metal-based cellular materials greatly enrich the family of ultralight materials and extend their applications with further reduced density. However, no insulating ultralight material better than silica aerogel has been reported since the 1930s. What is more, with reduced density, existing ultralight porous materials always have poor mechanical performance and thermal stability not up to 600 °C.[11−14] This largely limited their applications under high temperature conditions in modern industry.

Hexagonal boron nitride (BN), with similar atomic structure to graphene, shows distinct properties such as insulation with dielectric constant of 2.0−4.0[15] and significantly higher thermal and chemical stability.[16] However, synthesis of BN-based material is much more difficult than its carbon cousin mainly because of the binary nature of hexagonal BN and the limitation in B−N source. Until recently, few layer BN films were able to be fabricated, and the obtained films show excellent insulating property, thermal and chemical stability, and desirable mechanical properties.[17,18] Its smooth surface, similar lattice constant, and atomic layer thickness make it an appealing dielectric to complement graphene devices.[19−21] BN-based ultralight materials should be of great potential for novel applications but remain challenged to be fabricated. In this paper, we present a method for fabrication of free-standing BN foams with three-dimensional hollow-tube-like networks and ultralow density of 1.6 mg/cm^3. The BN foam consists of five hierarchical structural levels and exhibits excellent thermal stability in oxygen environment as well as superelastic and robust ultralow permittivity comparable to that of air.

The BN foam was grown on a nickel foam template by low-pressure chemical vapor deposition (CVD) using solid borazane as the precursor. Typically, a quartz container loaded with 0.5 g of borazane powder was heated up to around 100 °C to generate borazane vapor, which diffused into a quartz tube furnace at 1000 °C and formed BN film on the surface of nickel skeleton due to polyreaction, cross-linking, and dehydrogenation reaction process.[22,23] In this process, borazine was first converted to polyborazylene, which diffused onto the surface of Ni foam and underwent a cross-linking reaction of B−H and N−H groups on adjacent chains; finally, the unaligned chain branches of polyborazylene were dehydrogenated and ultimately formed the hexagonal BN.[22,23] After the growth of BN, the color of the Ni foam changed from shiny white to dark gray (see Figure S1). To isolate the BN foam from the nickel skeleton without damage or collapse, a thin layer of poly(methyl methacrylate) (PMMA) was dip-coated on the BN surface before removing the nickel template. After the

Received: April 12, 2013
Revised: June 24, 2013
Published: June 25, 2013

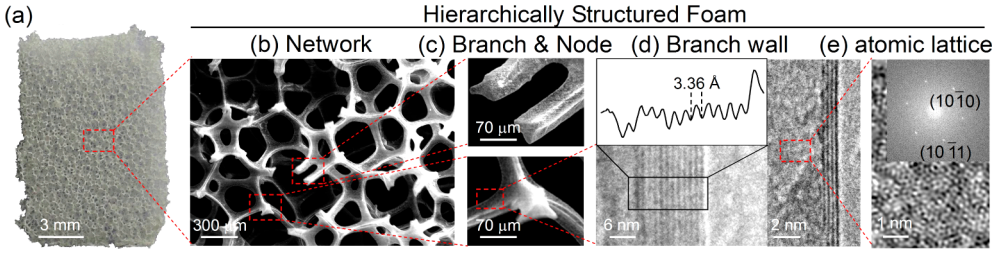

Figure 1. Hierarchical structures of the free-standing BN foam. (a) Photograph of a free-standing BN foam. (b) SEM image of a BN foam network. (c) Magnified SEM images of two branches and a node. (d) High-resolution TEM images of BN sheets near their folded edges, where the number of dark lines for the edges indicates the thickness of 12 and 4 layers, respectively. The interlayer spacing obtained from the edges is ~0.34 nm. (e) High-magnification TEM image and its fast Fourier transform (inset), indicating the typical hexagonal lattice of the BN sheet.

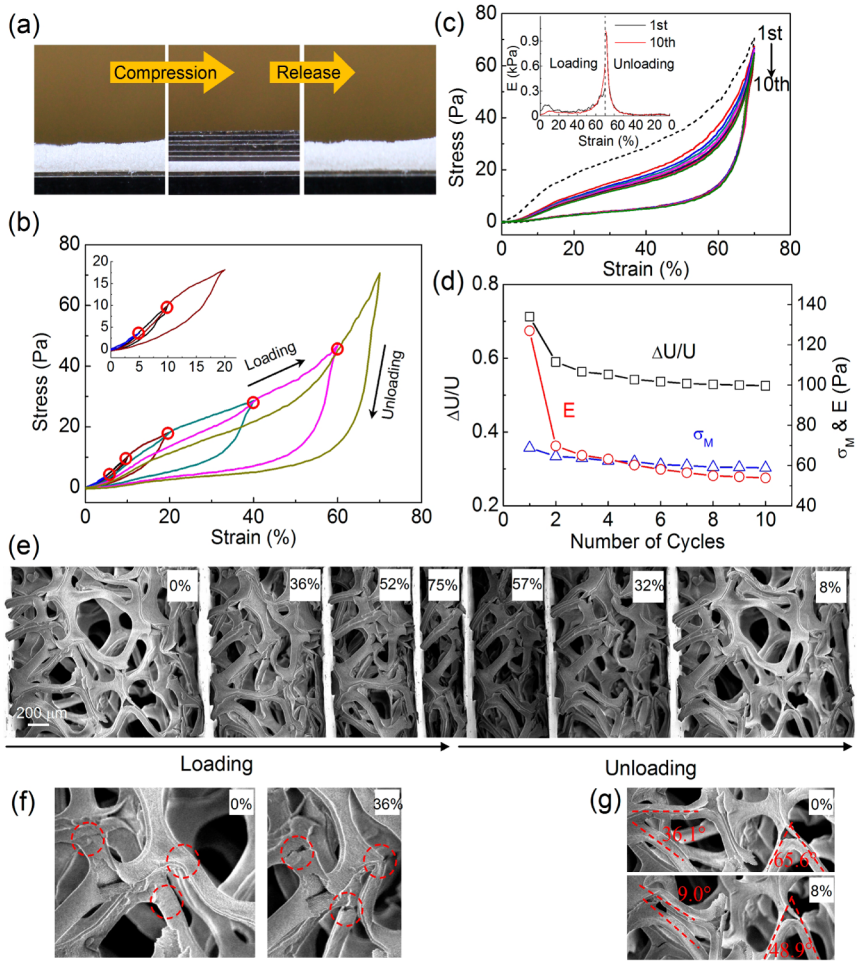

Figure 2. Mechanical properties of the BN foam. (a) Optical photographs showing the BN foam recovers its original shape after compression of ~70%. (b) Stress–strain curves for the BN foam during loading–unloading cycles in sequence of increasing strain amplitudes. In the compression process, the curve intersects with the last curve at the maximum strain point of the last loading, as labeled by the red circles. The insert is enlarged curves for cycles with 5%, 10%, and 20% maximum strain. (c) Fatigue resistance of BN foam to cyclic compression to 70% strain. Inset: evolution of the tangent modulus of the BN foam in the first and tenth compression cycles, respectively. (d) History of the maximum stress (σ_M), compressive modulus (E), and energy loss ratio during the 10 cycles shown in (c). (e) *In situ* SEM images of the BN foam under different strains in one compression cycle with maximum strain of 75%. (f) Cracks formed during compression. (g) Residual buckling deformation at nodes after compression to 75%.

nickel skeleton being etched by HCl solution, the PMMA layer was then removed by heating the BN/PMMA in air at 700 °C for 1 h. This simple method avoids the complicated supercritical drying process usually adopted in aerogel production and the use of liquid solvent, such as acetone.[2] The free-standing BN foam (Figure 1a) obtained by this method copies the structure of the nickel foam template perfectly and shows five hierarchical orders: foam-like macrostructure, network with hole size of hundreds of micrometers (Figure 1b), hollow-tube-like branches and nodes at tens of micrometers (Figure 1c), branch wall consisting of a few to over ten BN layers (Figure 1d), and atomic lattice of hexagonal BN (Figure 1e). Four branches with triangle cross section (see Figure S2) are connected to each node. For the TEM image

dx.doi.org/10.1021/nl401308v | *Nano Lett.* 2013, 13, 3232–3236

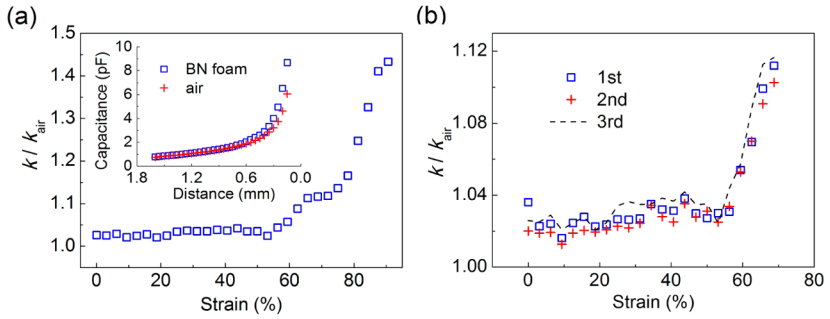

Figure 3. Permittivity of the BN foam. (a) Ratio of the dielectric constant of the BN foam at 100 kHz to that of air as a function of the strain. (b) Permittivity of the BN foam relative to air as a function of strain in two compressing cycles to 70% strain and the third cycle shown in (a).

shown in Figure 1d, the BN branch walls are scrolled at the edges where the BN layers are locally parallel to the electron beam and exhibit dark lines with higher contrast, providing a clear TEM signature for the number of BN layers. The measured average interlayer distance of the BN branch walls is about 0.336 nm, consistent with the *c*-axis spacing of h-BN.[24] The fast Fourier transform of the high-magnification image taken from the central part gives spot arranged in a typical hexagonal pattern (inset of Figure 1e), and the interplanar spacings deduced from the diffraction pattern are found to be consistent with the structure of hexagonal BN (ICSD Card No. 027986). The hexagonal BN structure is also confirmed by the Raman spectrum (see Figure S3).[25] Energy-dispersive X-ray spectroscopy analysis further shows that the foam contents pure BN layers (see Figure S4). No peak of C or Ni was found in the X-ray spectrum, indicating fully removing of the Ni template and PMMA support. Contributed to the large size of the holes and hollow-tube-like branches with thin wall, the BN foam is ultralight with a density of only 1.6 mg/cm^3. The corresponding volume fraction of the BN foam is around 0.076%. Although the yielding porosity is reckoned >99.9%, the BN foam is structurally stable. No collapse and shrinkage was found after removing the nickel template, in sharp contrast to the unstable 3D graphene networks which collapse after removing the template and PMMA support.[7] We attribute this structural stability to the unique hollow branch structure, which utilizes the material with balanced rigidity and elasticity, and the absence of solvent surface tension when removing the PMMA.

As can be expected by its high porosity, the BN foam can be extensively compressed. However, it is surprising that the BN foam exhibits complete recovery even after compression up to 70% as shown in Figure 2a, especially in comparing with the collapsed graphene foam with similar structures. We further measured the compressive stress σ as a function of strain ε. Figure 2b presents the $\sigma-\varepsilon$ curves of six compression cycles with strain amplitude of 5%, 10%, 20%, 40%, 60%, and 70% in sequence. It is interesting that each succeeding loading curve exactly rises back to the maximum stress−strain point of the preceding cycle and continues the trend of the preceding loading curve in the full range of our measurements, showing a perfect strain memory effect.

We adopt the envelope line of these $\sigma-\varepsilon$ curves in Figure 2b as the first compression curve directly up to 70% strain and conducted consecutive compression cycles to characterize the stability of the cyclic resilient property. The $\sigma-\varepsilon$ curves are shown in Figure 2c (see Figure S5 for each of these $\sigma-\varepsilon$ curves). Curves of the loading process shows three distinct regions typically observed in elastomers[26] and metallic microlattices[27] including a initial Hookean region at 4% < ε < 11%, a plateau at 11% < ε < 50%, and final densification with rapidly increasing stress, as shown by the evolution of the tangent modulus in the compression cycle (the inset of Figure 2c). The initial increase of the tangent modulus in the range of ε < 4% is attributed to the increase of contact area between the sample and the pressure head. The primary deformation in the Hookean region is linear elastic dominated by bending. The plateau is mainly attributed to the postbuckling deformation of the branches and nodes. At large strain, the opposing cell walls come into touch each other. Upon unloading, the stress drops rapidly with decreasing strain to 60% but does not vanish until the strain is approaching zero, indicating the complete recovery of the BN foam. Thus, similar to most resilient cellular materials,[4−6,9,10,27,28] hysteresis loops are found in the loading−unloading cycles, which indicate energy dissipation that can be attributed to the buckling and kinking of microstructures; the friction and adhesion between branches and the cracks especially happened in the first compression for the large dissipation. At 70% strain amplitude, the energy loss coefficient ($\Delta U/U$) for the first cycle is estimated to be around 71% and then diminishes with cycle number and tends to stable around 52% after the fourth cycle. The maximum stress (σ_M) and the elastic modulus (E) show the same tendency (Figure 2d). Compared with other ultralight materials, BN foam preserves the lowest elastic module of 70−127 Pa, several orders lower than most ultralight materials (see Table S1), showing its potential application in force sensor.

Compression exceeding 70% strain can introduce permanent residual deformation that cannot recover. To reveal the origination of the residual deformation and explore the mechanism of the strain memory effect as well, we determined the structure reorganization of the BN foam in a whole loading−unloading cycle via *in situ* SEM imaging normal to the compression direction, as shown in Figure 2e. After a 75% compression, an 8% residual deformation can be observed. Under compression, the strain mainly embodies in the twist of the branches around the nodes. Thus, larger stress concentration was introduced at the nodes, and some microcracks originated, as shown in Figure 2f. These microcracks reduce the elastic modulus at the Hookean region of the succeeding cycle and also depress the stress until the experienced maximum strain approached, at which the state of BN microstructure is almost as the same as that of the preceding maximum compressed BN, explaining the strain memory effect. Residual buckling and wrinkles are also found around the nodes after removing the loading, as indicated in Figure 2g, accounting for the permanent residual strain.

dx.doi.org/10.1021/nl401308v | *Nano Lett.* 2013, 13, 3232−3236

The intrinsic electric insulation of h-BN and high porosity make the BN foam a promising material with ultralow permittivity. We determined its permittivity relative to air at 100 kHz under different compressive strain by measuring the capacitance of a parallel-plate capacitor with controlled distance filled by the BN foam. As shown in the inset of Figure 3a, the capacitance of the air separated capacitor is proportional to the reciprocal of the distance. At distance larger than 0.7 mm, the capacitance of the BN foam separated capacitor remains close to that of the air but then increases more quickly with further reduction in distance, indicating increase in the permittivity. The deduced permittivity of the BN foam relative to air is shown in Figure 3a. It increases slightly from 1.026 under strain-free state to 1.044 at 56.3% strain. Then the permittivity increases remarkably with increasing strain beyond 60%. However, even for BN foam at 90.6% strain, its permittivity relative to air is only 1.43. As can be expected from the excellent resilience property of the BN foam, the measured relative permittivity−strain curves for the first two consecutive compressing cycles to 70% strain amplitude and the succeeding third cycle shown in Figure 3a are nearly the same as shown by Figure 3b (see Figure S6 for the capacitance−strain curves).

Thermogravimetric analysis showed that the weight of the BN foam kept stable in oxygen environment up to 1200 °C (see Figure S7), inheriting from the stability of h-BN.[29] This thermochemical stability is significantly higher than that of carbon-based materials, such as carbon nanotube and graphene which start to be oxidized at temperature around 600 °C.[11,12,14] As all our samples for testing are preheated at 700 °C in air for 1 h, the static as well as cyclic mechanical and dielectric properties of the BN foam should be stable at least up to 700 °C. In comparing, the structure of silica aerogels can only be stable up to 500 °C.[30] Vividly, a piece of such ultralight and highly thermal stable BN foam can be lift-up without burn-up in the hot flame of a spirit lamp (see Figure S8).

In summary, we have fabricated BN foam with novel properties by CVD using nickel foam as template. The free-standing BN foam consists of interconnected hollow-tube-like branches without collapse and brings all the fascinating properties such as ultralightness, superelasticity, exceptionally thermal stability, and ultralow permittivity, with each of them comparable to or surpassing the optimal one of existing ultralight materials (see Table S1). Most importantly, the permittivity of the BN foam remains comparable to that of air over a large strain range, showing great potential for wide applications such as tunable capacitors at elevated temperature.

■ ASSOCIATED CONTENT

Supporting Information

Method details, Figures S1−S8, and Table S1. This material is available free of charge via the Internet at http://pubs.acs.org.

■ AUTHOR INFORMATION

Corresponding Author

*Tel +86 25 84891896; e-mail wlguo@nuaa.edu.cn (W.G.).

Notes

The authors declare no competing financial interest.

■ ACKNOWLEDGMENTS

We thank L. T. Sun of the Southeast University for the TEM characterization. This work was supported by 973 program (2013CB932604, 2012CB933403), the National NSF (91023026, 51002076) of China, Funding of Jiangsu Innovation Program for Graduate Education (CXLX12_0136), Funding for Outstanding Doctoral Dissertation in NUAA (BCXJ12-02), and the Fundamental Research Funds for the Central Universities.

■ REFERENCES

(1) Miller, R. D. *Science* **1999**, *286* (5439), 421−423.
(2) Kistler, S. S. *Nature* **1931**, *127* (3211), 741.
(3) Guinness Book of World Records, Least Dense Solid, 2003; www.guinnessworldrecords.com/records-1/leastdense-solid/.
(4) Kim, K. H.; Oh, Y.; Islam, M. F. *Nat. Nanotechnol.* **2012**, *7* (9), 562−566.
(5) Gui, X.; Wei, J.; Wang, K.; Cao, A.; Zhu, H.; Jia, Y.; Shu, Q.; Wu, D. *Adv. Mater.* **2010**, *22* (5), 617−621.
(6) Mecklenburg, M.; Schuchardt, A.; Mishra, Y. K.; Kaps, S.; Adelung, R.; Lotnyk, A.; Kienle, L.; Schulte, K. *Adv. Mater.* **2012**, *24* (26), 3486−3490.
(7) Chen, Z.; Ren, W.; Gao, L.; Liu, B.; Pei, S.; Cheng, H. *Nat. Mater.* **2011**, *10* (6), 424−428.
(8) Cao, X.; Shi, Y.; Shi, W.; Lu, G.; Huang, X.; Yan, Q.; Zhang, Q.; Zhang, H. *Small* **2011**, *7* (22), 3163−3168.
(9) Qiu, L.; Liu, J. Z.; Chang, S. L.Y.; Wu, Y.; Li, D. *Nat. Commun.* **2012**, *3*, 1241−1247.
(10) Schaedler, T. A.; Torrents, A.; Sorensen, A. E.; Lian, J.; Greer, J. R.; Valdevit, L.; Carter, W. B. *Science* **2011**, *334* (6058), 962−965.
(11) Yamamoto, M.; Einstein, T. L.; Fuhrer, M. S.; Cullen, W. G. *ACS Nano* **2012**, *6* (9), 8335−8341.
(12) Liu, L.; Ryu, S.; Tomasik, M. R.; Stolyarova, E.; Jung, N.; Hybertsen, M. S.; Steigerwald, M. L.; Brus, L. E.; Flynn, G. W. *Nano Lett.* **2008**, *8* (7), 1965−1970.
(13) Schmidt, M.; Schwertfeger, F. *J. Non-Cryst. Solids* **1998**, *225*, 364−368.
(14) Hata, K.; Futaba, D. N.; Mizuno, K.; Namai, T.; Yumura, M.; Iijima, S. *Science* **2004**, *306* (5700), 1362−1364.
(15) Kim, K. K.; Hsu, A.; Jia, X.; Kim, S. M.; Shi, Y.; Dresselhaus, M.; Palacios, T.; Kong, J. *ACS Nano* **2012**, *6* (10), 8583−8590.
(16) Golberg, D.; Bando, Y.; Huang, Y.; Terao, T.; Mitome, M.; Tang, C.; Zhi, C. *ACS Nano* **2010**, *4* (6), 2979−2993.
(17) Song, L.; Ci, L.; Lu, H.; Sorokin, P. B.; Jin, C.; Ni, J.; Kvashnin, A. G.; Kvashnin, D. G.; Lou, J.; Yakobson, B. I.; Ajayan, P. M. *Nano Lett.* **2010**, *10* (8), 3209−3215.
(18) Kim, K. K.; Hsu, A.; Jia, X.; Kim, S. M.; Shi, Y.; Hofmann, M.; Nezich, D.; Rodriguez-Nieva, J. F.; Dresselhaus, M.; Palacios, T.; Kong, J. *Nano Lett.* **2012**, *12* (1), 161−166.
(19) Dean, C. R.; Young, A. F.; Meric, I.; Lee, C.; Wang, L.; Sorgenfrei, S.; Watanabe, K.; Taniguchi, T.; Kim, P.; Shepard, K. L.; Hone, J. *Nat. Nanotechnol.* **2010**, *5* (10), 722−726.
(20) Xue, J.; Sanchez-Yamagishi, J.; Bulmash, D.; Jacquod, P.; Deshpande, A.; Watanabe, K.; Taniguchi, T.; Jarillo-Herrero, P.; LeRoy, B. J. *Nat. Mater.* **2011**, *10* (4), 282−285.
(21) Levendorf, M. P.; Kim, C.; Brown, L.; Huang, P. Y.; Havener, R. W.; Muller, D. A.; Park, J. *Nature* **2012**, *488* (7413), 627−632.
(22) Fazen, P. J.; Remsen, E. E.; Beck, J. S.; Carroll, P. J.; McGhie, A. R.; Sneddon, L. G. *Chem. Mater.* **1995**, *7* (10), 1942−1956.
(23) Shi, Y.; Hamsen, C.; Jia, X.; Kim, K. K.; Reina, A.; Hofmann, M.; Hsu, A. L.; Zhang, K.; Li, H.; Juang, Z. Y.; Dresselhaus, M. S.; Li, L. J.; Kong, J. *Nano Lett.* **2010**, *10* (10), 4134−4139.
(24) Mishima, O.; Era, K. *Electric Refractory Materials*; Marcel Dekker: New York, 2000.
(25) Gorbachev, R. V.; Riaz, I.; Nair, R. R.; Jalil, R.; Britnell, L.; Belle, B. D.; Hill, E. W.; Novoselov, K. S.; Watanabe, K.; Taniguchi, T.; Geim, A. K.; Blake, P. *Small* **2011**, *7* (4), 465−468.
(26) Gibson, L. J.; Ashby, M. F. *Cellular Solids Structure and Properties*; Cambridge University Press: Cambridge, 1997.
(27) Torrents, A.; Schaedler, T. A.; Jacobsen, A. J.; Carter, W. B.; Valdevit, L. *Acta Mater.* **2012**, *60* (8), 3511−3523.

(28) Suhr, J.; Victor, P.; Ci, L.; Sreekala, S.; Zhang, X.; Nalamasu, O.; Ajayan, P. M. *Nat. Nanotechnol.* **2007**, *2* (7), 417−421.
(29) Jacobson, N.; Farmer, S. *J. Am. Ceram. Soc.* **1999**, *82* (2), 393−398.
(30) Aranda, L. L. *Potentials, IEEE* **2001**, *20*, 12−15.